The Influence of Strain Hardening and Strain-Rate Sensitivity on Sheet Metal Forming

A. K. GHOSH

Research Laboratories, General Motors Corp., Warren, Mich.; Presently, Science Center, Rockwell International, Thousand Oaks, Calif.

The current understanding of sheet metal stamping processes is discussed in the light of materials' ability to distribute plastic strains in uniaxial and biaxial deformation. The focus is on the plastic flow properties, namely strain hardening and strain-rate sensitivity. Distribution of strain from uniaxial tensile specimens and sheets stretched over a rigid punch are presented for a number of sheet materials to illustrate the importance of these properties. Some effects of deformation rate are also presented.

Introduction

The most common mode of failure in cold-forming of sheet metal components is the development of a localized (through-thickness) neck or tear [1, 2],[1] which occurs generally over a punch radius as the sheet surface area is increased to conform to the punch shape. The problem is one of distributing deformation uniformly throughout the sheet, since a punch radius acts as a strain-concentrator, by virtue of its curvature and frictional resistance [3, 4]. A peak develops in the strain distribution and ultimately produces a neck or tear. Success in manufacturing is, therefore, directly related to (i) the material's ability to distribute strain more uniformly under an externally applied stress-gradient, and (ii) the strain limits that can be tolerated prior to the development of a neck[2] or tear. As illustrated schematically in Fig. 1, to successfully make a flat circular cup depends upon achieving the required length of line ABCD (given by the area under the strain distribution curve SS') without reaching the forming limit. A poorer distribution of strain FF' causes the peak strain to reach the forming limit earlier and failure results.

Gentler tool curvature and increased lubrication reduce the external stress gradient. For a given external stress gradient, however, a material's inherent ability to distribute strain coupled with its forming limit determine its overall formability. Although the contribution of these two elements change in a complex manner with the nature of the external stress-gradient, the purpose of this paper is to examine their dependence only on the material properties, namely the hardening and softening processes occurring during deformation. In the material to follow, the influence of the hardening properties on strain gradients, the necking phenomenon and detailed strain distributions are examined for both uniaxial and biaxial deformation. Finally, the influence of the rate of deformation on the necking process and overall formability is discussed.

Sources of Hardening. The two primary sources of hardening during deformation are: (i) strain hardening, and (ii) strain-rate hardening. A simplified consitutive description is given by [5]

$$\sigma = K\epsilon^n\dot{\epsilon}^m \tag{1}$$

where, K = constant, n = strain hardening exponent, and m = strain-rate hardening exponent. ($n \to 0$ for superplastic material, while $m \to 0$ for most ductile metals at room temperature.) In a workpiece, the region undergoing thinning strain-hardens and becomes resistant to further deformation, and thereby forces the deformation to the less deformed neighboring elements. Similarly, as local strain-rate increases in areas undergoing thinning, the strain-rate hardening of such regions forces deformation to occur in areas experiencing a slowdown in the rate of deformation. Both processes thus resist strain localization.

Uniaxial Deformation

Influence on Strain Gradients. Metal deformation is always accompanied by gradients in plastic strain and strain-rate. In a carefully machined tensile specimen, such gradients, which are initially small, begin to grow with deformation. Considering a specimen of homogeneous material, strain gradient can be determined from the gradient in cross-sectional area initially present. Since the load, $P(x)$, at any location x is given by

$$P(x) = \sigma(x)A(x) \tag{2}$$

using equation (1) for stress, $\sigma(x)$, and expressing the cross-sectional area, $A(x)$, in terms of the original area, $A_0(x)$, one obtains

[1] Numbers in brackets designate References at end of paper.

[2] A diffuse neck developed in a sheet tensile specimen is regarded as acceptable, while a through-thickness neck (or shear band) that appears subsequently is objectionable.

Contributed by the Materials Division for publication in the JOURNAL OF ENGINEERING MATERIALS AND TECHNOLOGY. Manuscript received by the Materials Division July 6, 1976; revised manuscript received September 27, 1976.

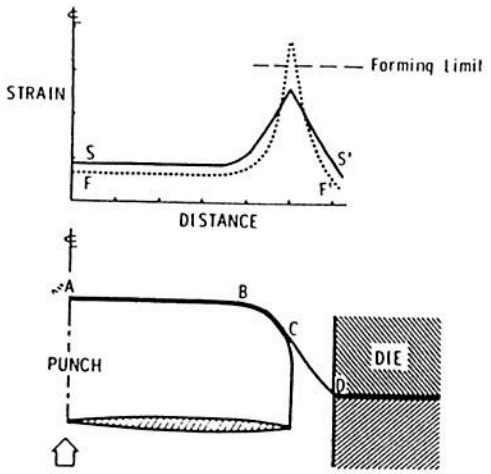

Fig. 1 Schematic radial strain distribution for punch forming of a flat cylindrical cup. The area under the strain distribution curve SS' equals the length of line ABCD and represents a successful part, while FF' produces a visible neck.

$$P(x) = K[\epsilon(x)]^n[\dot{\epsilon}(x)]^m A_0(x) \exp[-\epsilon(x)] \quad (3)$$

Now, differentiating equation (3) with respect to x and setting $dP/dx = 0$ for constancy of pulling load along x axis, the strain gradient can be expressed as

$$(-d\epsilon/dx) = \frac{1}{(n/\epsilon) - 1}\left[(1/A_0)(dA_0/dx) + (m/\dot{\epsilon})(d\dot{\epsilon}/dx)\right] \quad (4)^3$$

Thus, the strain gradient depends on three quantities: (i) A strain hardening factor, $1/((n/\epsilon) - 1)$, (ii) the gradient, $(1/A_0)(dA_0/dx)$, in the original area, and (iii) the strain-rate gradient term, $(m/\dot{\epsilon})(d\dot{\epsilon}/dx)$. Step-by-step computation is necessary to determine this last term. The dependence of strain gradient on ϵ/n for an arbitrary value of $(1/A_0)(dA_0/dx) = 10^{-4}$/mm is shown in Fig. 2. For a fixed value of n, $-d\epsilon/dx$ is found to increase rapidly with ϵ; while for a fixed ϵ, $-d\epsilon/dx$ decreases with increase in n. When $m > 0$, the quantity within brackets in equation (4) decreases since $d\dot{\epsilon}/dx$ becomes increasingly negative with deformation. This slows the rate of increase of $-d\epsilon/dx$, and if m is sufficiently large (as in superplastic deformation) the strain gradient remains relatively low.

The case of $m < 0$ is more complex. During deformation $d\dot{\epsilon}/dx$ can periodically change sign (as long as $n > 0$) as strain-rate softening is offset by strain hardening in order to maintain load equilibrium [7]. A similar change in the sign of $d\epsilon/dx$ occurs during dynamic strain aging in various solid solution alloys and results in the characteristic serrated flow behavior [8].

Influence on Tensile Necking. The relatively slight gradients in strain and strain-rate in a tensile specimen begin to grow as deformation passes through the load maximum. This occurs, as shown in Fig. 3(*a*), when the rate of hardening $(d\sigma/d\epsilon)$, while decreasing during deformation, comes to a balance with the increasing flow stress (σ). As is well known, when $m = 0$ and strain hardening follows a power law, this occurs at $\epsilon = n$. Since strain gradients are extremely small up to this point, n provides a measure of uniform strain (ϵ_u) and marks the onset of diffuse necking. Further deformation is diffusely unstable (or quasi-stable) as it occurs under steadily falling load. Strain continues to localize with eventual formation of a thickness neck occurring when $d\sigma/d\epsilon = \sigma/2$, i.e., at $\epsilon = 2n$ for power law hardening materials $(m = 0)$ [9].

Since $d\dot{\epsilon}/dx$ is small up to the maximum load, even large values of m do not appreciably increase the uniform strain (Fig. 3(*b*)). Beyond this point, however, $d\dot{\epsilon}/dx$ rises enough to cause a strain-rate induced flow stress increase, with an even greater increase in $d\sigma/d\epsilon$. The rate of stability loss is thereby reduced and local necking condition is not satisfied until strains are greater than $2n$. As predicted from equation (4) (also shown in Fig. 2), a smaller $-d\epsilon/dx$ is maintained throughout this stage, and necking may not be visually apparent until considerable extension has accumulated in the specimen. Even though this deformation is quasistable in nature, it is practically "uniform" and useful.

An analysis of stability loss during diffuse necking was made

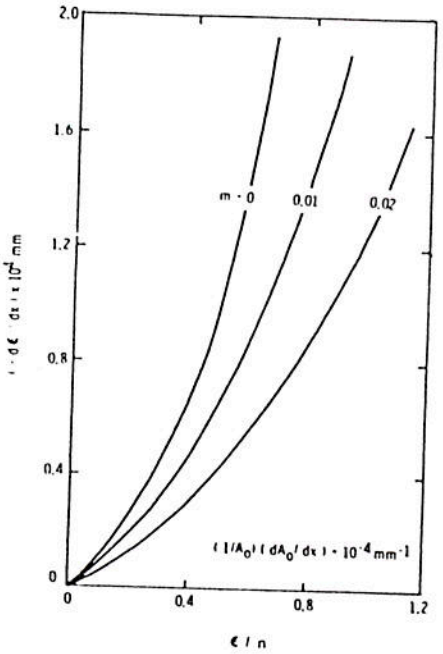

Fig. 2 The growth of strain gradient $(-d\epsilon/dx)$, as a function of (ϵ/n) is shown for various values of m

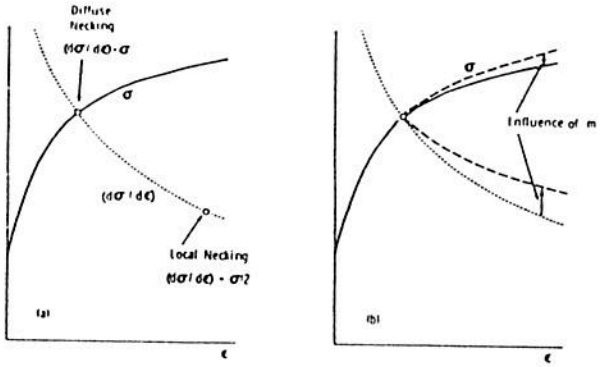

Fig. 3 Schematic plots of true stress and strain hardening rate as functions of true strain (Considére construction): (*a*) For $m = 0$, diffuse necking begins when $(d\sigma/d\epsilon) = \sigma$, and local necking when $(d\sigma/d\epsilon) = \sigma/2$; (*b*) For $m > 0$, diffuse instability strain is relatively unaffected, while σ and $(d\sigma/d\epsilon)$ change appreciably beyond this point to increase the local necking strain.

[3] As strain gradient becomes appreciable, the maximum principal stress direction everywhere in the specimen no longer remains parallel to the tensile axis and equations (3) and (4) must be modified to include the nonparallel components (as will appear in reference [6]).

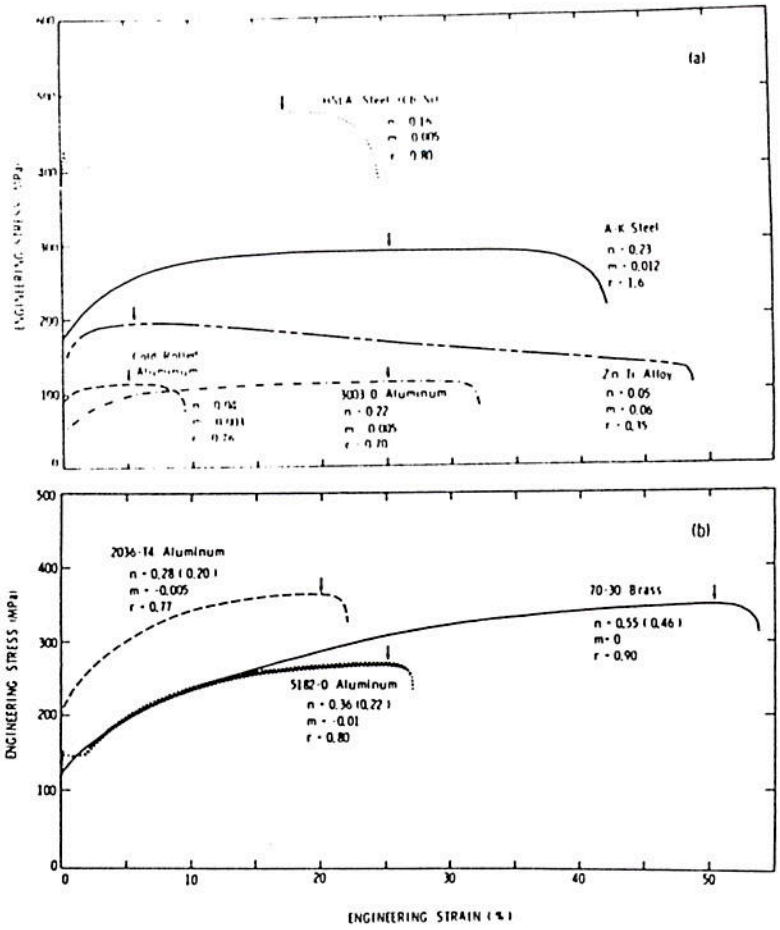

Fig. 4(a and b)

Fig. 4 Engineering stress-strain curves in uniaxial tension for a number of test materials (data from references [4, 10, 12, 18, 26]): (a) materials with $m > 0$, (b) materials with $m \leq 0$. Maximum load point is indicated by a short vertical arrow. (c) Post-uniform elongation, i.e., engineering strain occurring beyond maximum load, is plotted for the above materials as a function of m. Data for 5182-0 Aluminum at 150°C has been added from reference [11].

in reference [10], and it was found that even a small m can produce quasistable flow (with a nearly constant maximum load) over an appreciable strain range. Fig. 4(a) compiles some of these data. Low carbon steels (aluminum-killed or rimmed variety) with m as low as 0.01–0.016 (at quasistatic speed), can postpone the onset of localized necking and accumulate large amounts of post-uniform strain to account for nearly 40 percent of its total elongation to failure[4] (measured over 50.8 mm gage length). In 3003-0 aluminum ($n \sim 0.23$, $m \sim 0.005$), nearly 22 percent of the total elongation comes from beyond the maximum load, while in high strength low alloy (HSLA) steel ($n \sim 0.16$, $m \sim 0.008$), this is approximately 30 percent. In dispersion hardened zinc ($n \sim 0.05$, $m \sim 0.06$), nearly 90 percent of the elongation is post-uniform, and although its m is small compared to superplastic alloys, the deformation characteristics are similar. Even cold-rolled aluminum in Fig. 4(a) derives 50 percent of its extension from beyond the maximum load ($m = 0.003$).

In materials exhibiting serrated flow or negative m, on the other hand, deformation rapidly localizes beyond maximum load (Fig.

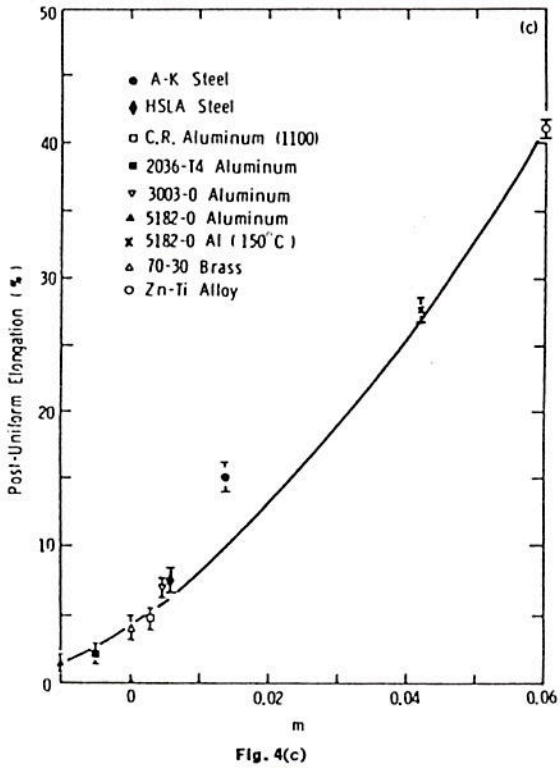

Fig. 4(c)

[4]The plastic anisotropy parameter (r) also influences the post-uniform deformation through its influence on flow stress in the neck as the local stress-state changes [10]. This effect is greater for larger values of r [0], and explains the somewhat larger post-uniform elongations of A-K steel ($r \sim 1.7$) in comparison to rimmed steel ($r \sim 1.0$).

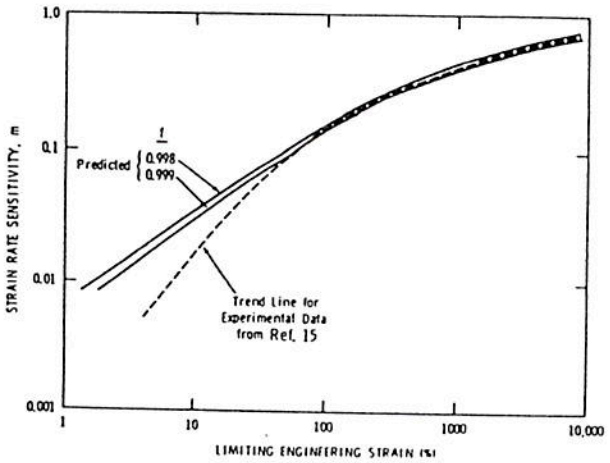

Fig. 5 The dependence of limiting engineering strain, upon localization of deformation in a neck from imperfection sizes (1-f) = 0.001, 0.002, calculated by using equation (5) for $n = 0$, is shown as a function of m (for large values of m, limiting engineering strain itself equals total elongation.) Trend line for experimental data from reference [15] is superimposed.

4(b)). Despite respectable strain-hardening properties, brass ($n = 0.55$) and aluminum alloys ($n = 0.28$ for 2036-T4, $n = 0.36$ for 5182-0) show small post-uniform extension because m is either zero (brass) or slightly negative (-0.005 for 2036-T4 and -0.01 for 5182-0 aluminum). The post-uniform elongations for materials in Figs. 4(a) and (b), and 5182-0 aluminum at 150°C (from reference [11]) are plotted as a function of m in Fig. 4(c), clearly indicating a monotonic dependence. The somewhat greater elongation for A-K steel is believed to be a result of (i) its high value of r, and (ii) an increased effective strain hardening in the neck as the local stress-state changes [12]. While the functional dependence of Fig. 4(c) is complex, at elevated temperature (generally as m increases and n decreases) the flow is primarily controlled by m and the post-uniform elongation nearly equals the total elongation. For such cases, a growth model of an initial specimen imperfection (assumed to be a variation in cross-sectional area) predicts [13, 14] the dependence of engineering strain at failure, e^*, as

$$e^* = (1 - f^{1/m})^{-m} - 1 \tag{5}$$

where, f = 1 − (fractional size of imperfection (~0.001–0.002)). A plot of this prediction is compared in Fig. 5 with the trend line of data for a large number of materials from reference [15]. The agreement for large m (i.e., low n) is found to be remarkably good, while equation (5) does not directly apply to the lower m (i.e., higher n) materials.

Influence on Strain Distribution. The influences of n and m on, respectively, the uniform and post-uniform elongations become obvious upon examining the distribution of axial strain from failed tensile specimens of the materials shown in Figs. 4(a) and (b). Measured with a 0.50 mm square grid, these strain distributions are shown in Figs. 6(a) and (b). The interesting feature in Fig. 6(a) is that the diffuse neck is well-defined and small (for $m \leq 0$), outside of which the strain is nearly uniform. On the other hand, for $m > 0$ in Fig. 6(b), the neck region is diffuse and broad and strain drops continuously from its peak value without ever attaining a uniform value. Dispersion-hardened zinc is a good example. The post-uniform deformation is distributed outside the localized neck so gradually that an ex-

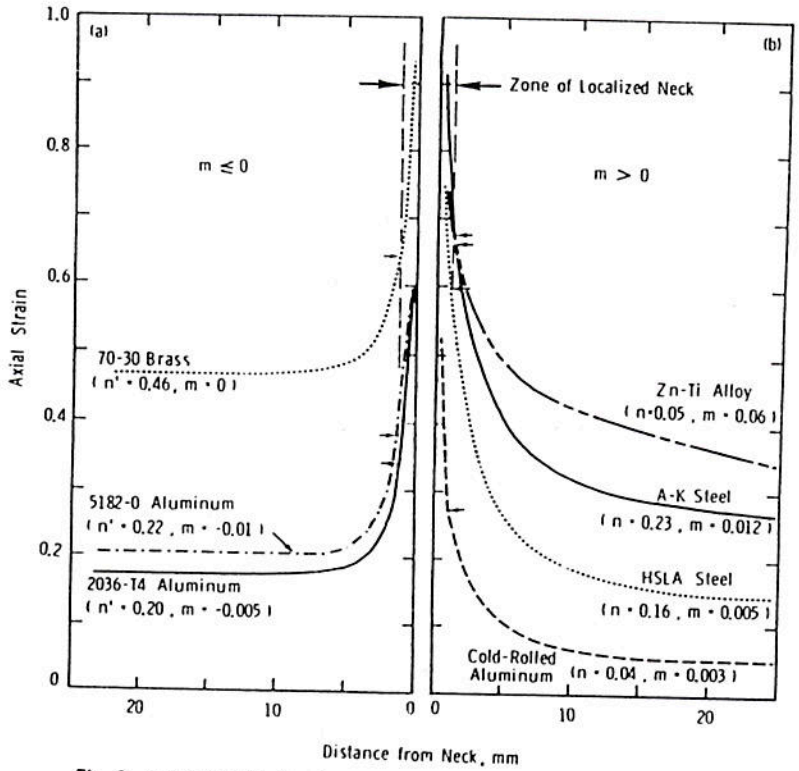

Fig. 6 Strain distribution in a tensile neck plotted as a function of distance from the center of neck: (a) for $m < 0$, (b) for $m > 0$. Sheet thickness ranges between 0.90 and 1.5 mm for which the zone of localized neck (visually determined) does not appreciably differ in size. The short horizontal arrows indicate the local necking strains.

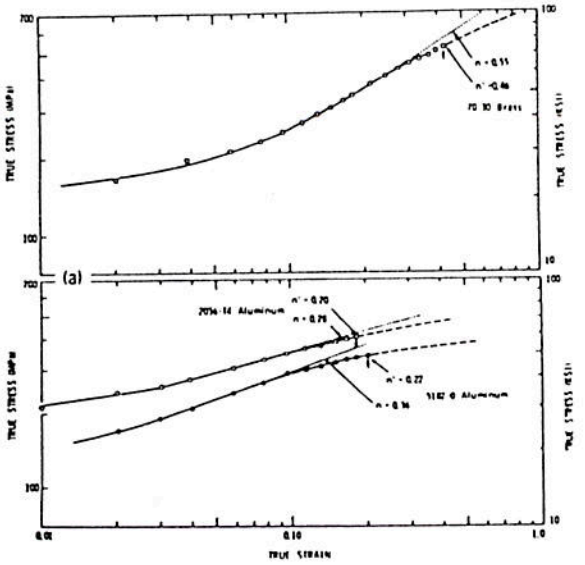

Fig. 7(a) Logarithmic plot of true stress versus true strain for 70:30 brass and the two aluminum alloys showing that the terminal value of the strain hardening exponent (n') is substantially less than the earlier constant value. These materials exhibit a three stage hardening behavior.

tremely long specimen would be required to capture the entire diffuse neck. For all practical purposes, a major part of the post-uniform flow thus becomes part of the "uniform" strain. In the case of dispersion-hardened zinc, this kind of strain could be as large as 0.35, while its n is only 0.05.

The zones of localized neck, determined visually, are nearly equal for these sheets of about the same thickness (0.9–1.5 mm). Short horizontal arrows indicating the limiting strains (immediately outside the localized neck) in Fig. 6(b) also show that local necking strains are significantly greater than $2n$ for these materials. The importance of a small m in conventional strain hardening materials just discussed is not commonly recognized. In contrast to this kind of behavior, however, Fig. 6(a) shows that uniform strains for brass and aluminum alloys are less than n and their local necking strains are less than $2n$. This effect is discussed more fully in the next paragraph.

Variation in n and m with Strain. The value of n, determined from the slope of the best linear fit through the log σ versus log ϵ data for brass, and 2036-T4 and 5182-0 aluminum alloys overestimates the strain-hardening exponent for strains near maximum load. Fig. 7(a) shows that a smaller n can be obtained on the basis of the last portion of the stress-strain data prior to maximum load. Clearly this terminal n value, designated as n', is related to maximum load condition and becomes equal to uniform strain, indicated in Fig. 6(a). Similarly, local necking strain becomes nearly equal to $2n'$. The reason for this drop in n immediately prior to the maximum load is unknown. One possible mechanism is the ease of cross slip leading to an exhaustion of strain hardening [16]. An additional effect may arise from strain-rate softening for materials with $m < 0$. Since the peak strain element is slightly advanced in strain and strain-rate compared to its neighbors, any strain-rate softening it may experience could cause an apparent loss in the rate of strain hardening.[5]

[5]While this terminal value of n is related to the necking event, a low value of n is also observed at small plastic strains (up to about 8-9% in mild steels) in most polycrystalline metals. Including this first stage, brass, 2036-T4 aluminum, 5182-0 aluminum, copper [17], austenitic stainless steel [17] and some HSLA steels [18] actually exhibit a three-stage hardening behavior, while mild steels and 3003-0 aluminum alloy and most HSLA steels do not show the third stage.

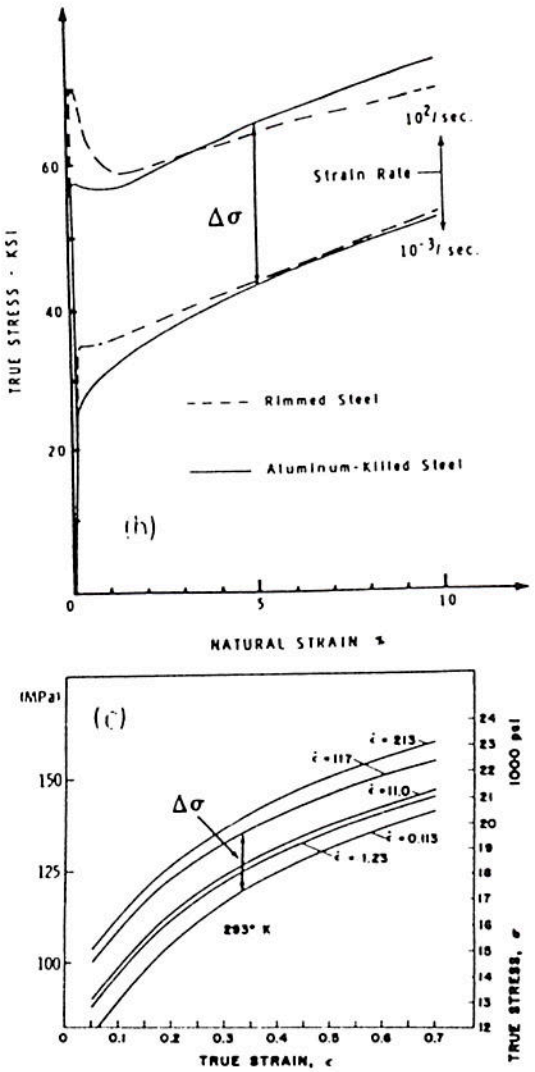

Fig. 7(b) The influence of tensile strain rate on stress-strain curves of mild steel (data from Green, et al. [19], and (c) similar results from constant true strain rate compression tests on 1100 aluminum (from Hockett [20]). A nearly constant $\Delta\sigma$ between the curves is observed.

Similar to the variation in n as a function of strain and its influence on ductility, the variations in m as functions of strain and strain-rate produce analogous results. Whiel m is nearly independent of strain for aluminum-killed and rimmed steels [19] (Fig. 7(b)), and pure aluminum at room temperature [20]

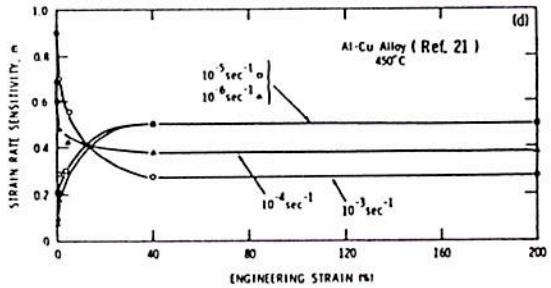

Fig. 7(d) The dependence of strain rate sensitivity upon engineering strain is an Al-Cu eutectic alloy at different rates of deformation (data from reference [21])

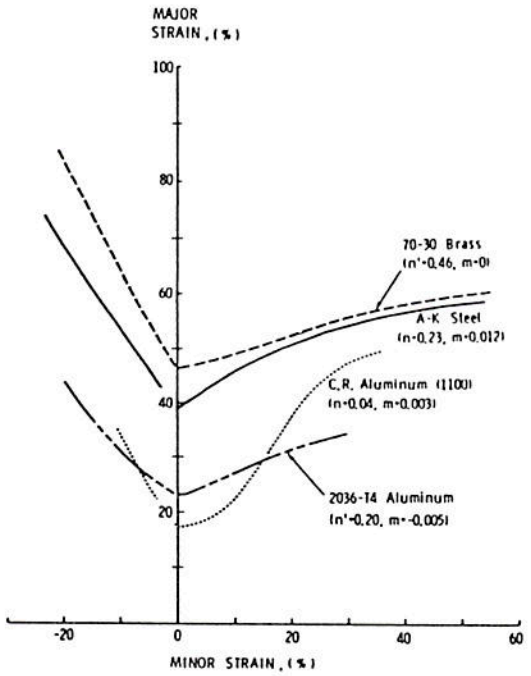

Fig. 8 The forming limit diagrams of 70:30 brass, A-K steel, cold-rolled aluminum and 2036-T4 aluminum from reference [25] and [26], determined by a punch stretching technique described in reference [25]. Engineering strains have been determined by 2.54 mm circle grids. The n and m values of the materials are shown here for comparison.

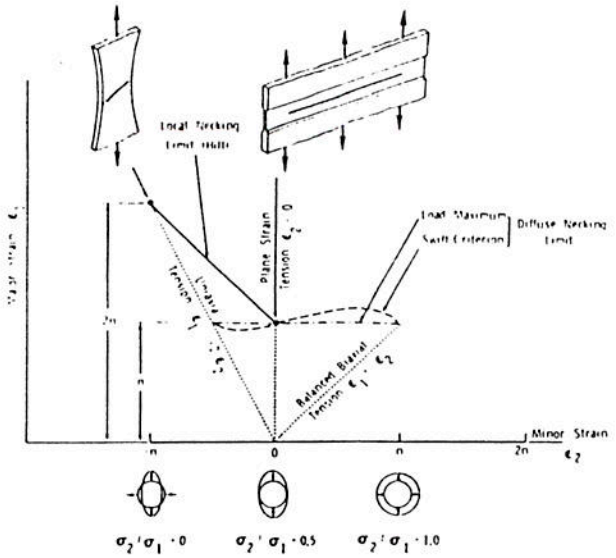

Fig. 9 Theoretical limiting major (true) strains are plotted as a function of minor (true) strain, within the range of uniaxial ($\sigma_2 = 0$) and balanced biaxial tension ($\sigma_2 = \sigma_1$). Diffuse necking limits are shown for two different (Swift [27] and Maximum Load) criteria (dashed lines), while local necking limit due to Hill [9] is shown for negative minor strains (solid line). Local necking was not predicted from these analyses.

(Fig. 7(*c*)), in the case of Cu-Al eutectics (at 450 C) [21] it has been shown that m increases with strain at low strain rates and decreases with strain at high rates. Equation (1) with a constant m is thus a poor approximation in many cases. A simultaneous drop in n and rise in m are observed with increasing deformation temperature in many materials[6] [21, 22], and a change in m as a function of strain is a common feature in such cases. It has been shown that the terminal value of m for such materials must be considered in order to relate to ductility. An overall constitutive description: $\sigma(\epsilon, \dot{\epsilon}, T)$, would however be more desirable in that case than isolated measurement of n and m.

Biaxial Deformation

Localized Necking: Forming Limit Concept. Forming a sheet metal component involves the application of biaxial loads in the sheet plane. Although the understanding developed for uniaxial deformation basically applies also to this kind of loading, the presence of an intermediate stress can significantly alter the strain level prior to the development of a localized neck. From an applications point-of-view, a localized neck constitutes failure and therefore, the dependence of local necking limit strain (commonly known as forming limit) on material properties is of great interest.

Originally developed by Keeler [23] and Goodwin [24] from mild steel production stampings, forming limit diagrams represent the major strain in the sheet surface at the onset of a visible neck as a function of minor strain. Fig. 8 shows the forming limit diagrams for a number of materials obtained from laboratory tests [25] involving stretching sheets over a hemispherical punch. The strain combinations below a given diagram indicate success while those above are failures (necking or tearing). (Deformation with positive minor strains is called stretch-type, and the negative minor strains indicate drawing-type action). These laboratory diagrams agree well with results from actual stampings; however, they are at a higher strain level than forming limits from in-plane deformation. The punch geometry and its frictional constraints influence the strain gradient and strain path to failure and are believed to be responsible for this effect [26]. The understanding of punch forming limits therefore must take these factors into account [3, 4]. It must be noted, in this connection, that an increased friction lowers formability primarily by increasing the strain concentration.

The classical plasticity predictions of local necking limits due to Hill [9] and diffuse necking limits due to Swift [27] are summarized in Fig. 9 for an isotropic, power-law hardening ($m = 0$) material under uniform, proportional strain paths. Within the range of stress-states between uniaxial and balanced biaxial tension, the Swift criterion (which is nearly the same as a maximum traction criterion) predicts that the diffuse necking strain is about n. On the other hand, Hill [9] identified localized necking (or shear band formation) with the attainment of a plane strain condition ($d\epsilon_2 = 0$). In the negative minor strain side there is a sheet direction with $d\epsilon_2 = 0$, and local necking strain drops from $2n$ in uniaxial tension ($d\sigma_1/d\epsilon_1 = \sigma_1/2$) to a value of n in plane strain tension ($d\sigma_1/d\epsilon_1 = \sigma_1$) (see Fig. 9). In reality there are always gradients in strain and strain-rate before localized necking. If $m > 0$, the strain limits would therefore increase on account of rate-induced hardening. For example, A-K steel ($m \sim 0.012$) exhibits an in-plane forming limit for the plane strain condition that is greater than n. Either increasing sheet thickness or decreasing punch radius raises these limits, particularly for $m > 0$. As shown in Fig. 8, the punch forming limit (plane strain) for A-K steel is greater than its n, while that for aluminum alloy is nearly equal to n.

In the biaxial stretching regime ($\epsilon_2 > 0$), however, localized necking is unexplainable by the Hill theory since no direction of zero length change exists in the sheet plane. A rationale for localized necking for $\epsilon_2 > 0$ was provided by Marciniak and Kuczynski [28] (M-K), who assumed that an inhomogeneity

[6] This is a typical characteristic of thermally activated (and time-dependent) deformation processes (within a certain temperature-strain rate regime), in which the importance of m increases with increasing temperature [22].

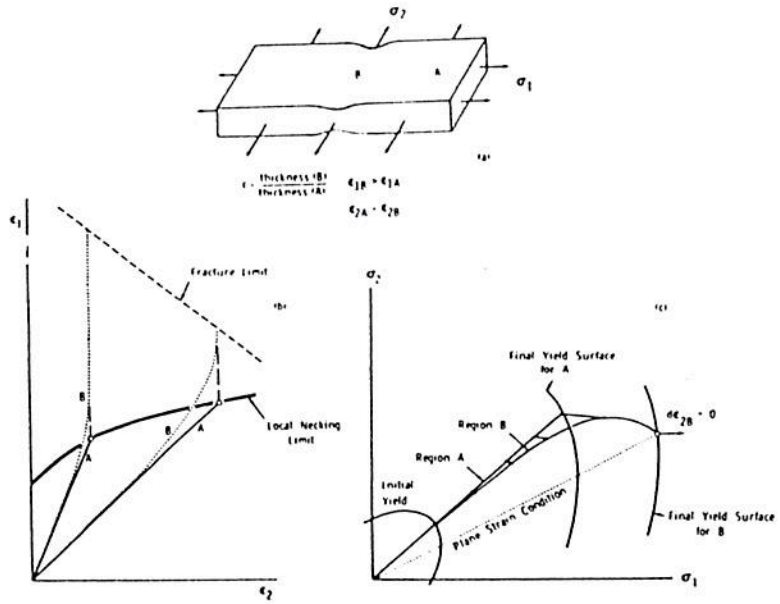

Fig. 10 (a) A region of inhomogeneity (thinned region, B) bounded by homogeneous material (A) undergoing biaxial stretching, according to the model of Marciniak and Kuczynski [28] (*b*) Proportional strain paths in region A (solid line) and those in region B (dashed line) are shown in biaxial strain space. When region B reaches the fracture limit curve, strain accumulated in region A defines the forming limit (localized necking). (c) The shift in stress-path in region B shown in biaxial stress-space is equivalent to the strain path change in (*b*). The attainment of plane strain state ($d\epsilon_{2B} = 0$) or fracture in region B signals the end of deformation for region A. This representation is after Sowerby and Duncan [29].

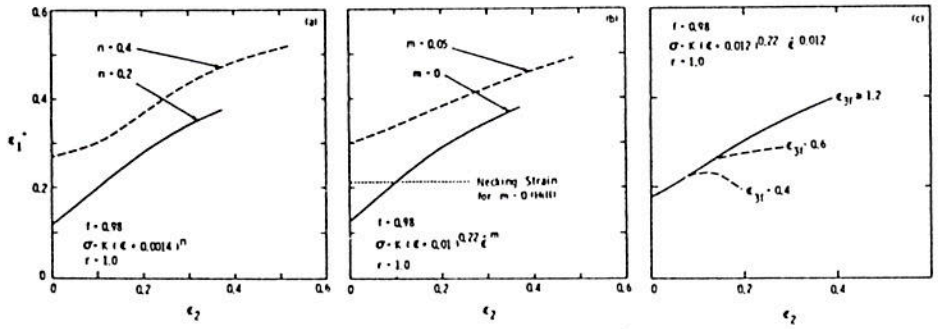

Fig. 11 The influence of (a) strain hardening exponent, (*b*) strain rate sensitivity, and (c) fracture strain on the forming limit diagram (for $\epsilon_2 > 0$), calculated from the model of Marciniak and Kuczynski. These data are from reference [13]. Note that any $f < 1.0$ produces plane strain limits less than n for $m \leq 0$. If $m > 0$, however, the plane strain limits could be substantially longer.

present in the material could be adequately modeled by a thinned trough-like region lying perpendicular to the direction of maximum principal stress (Fig. 10(*a*)). Compared to the surrounding material, the trough would thin faster under an imposed biaxial stress-state, i.e., ϵ_1 (trough) $> \epsilon_1$ (surroundings), while ϵ_2 (trough) $= \epsilon_2$ (surroundings). The strain path in the trough would turn toward plane strain and eventually reach fracture, as shown in Fig. 10(*b*). On the basis of an isotropic hardening theory of large plastic flow, the stress paths followed by the potential failure element [29] are illustrated in Fig. 10(*c*). From the basis of either stress path or strain path, the M-K analysis predicts an increasing forming limit with increasing biaxiality ($\epsilon_2/\epsilon_1 \rightarrow 1$); since as the imposed ϵ_2/ϵ_1 increases, the trough takes longer to reach a state of plane strain, thereby accumulating greater strain in the surrounding material.

The trends predicted by the M-K analysis agree, in general, with the experimental forming limit diagrams for various materials (Fig. 8). There are some quantitative disagreements, however, discussed in reference [26]. The general predictions [13] are illustrated in Figs. 11(*a*), (*b*), and (*c*). These are: (i) the level of the forming limit diagram is raised with increases in n and m, (ii) the rise is greater near plane strain than balanced biaxial tension, (iii) the fracture strain (indicated by ϵ_{3f}, i.e., thickness strain at fracture) can have a strong influence on the forming limit dingram near $\epsilon_2/\epsilon_1 = 1.0$. The last two observations mean that failure in plane strain is normally more "instability-controlled," while that near $\epsilon_2 = \epsilon_1$ is influenced more by fracture processes. The significance of a small m is realized from Fig. 11(*b*), which shows that the plane strain limits could indeed be greater than n (when $m > 0$) as observed in Fig. 8.

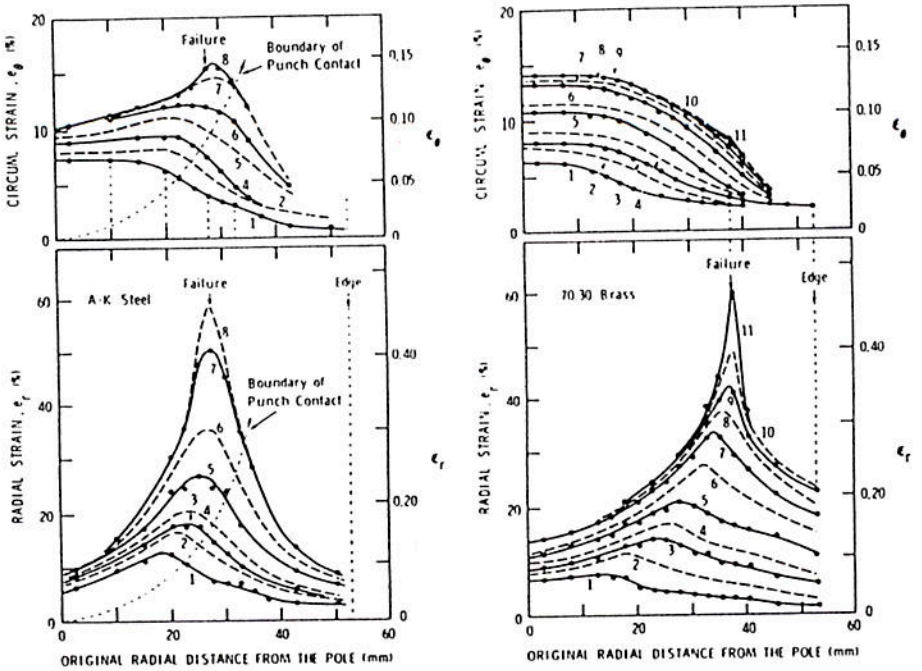

Fig. 12 Radial strain (e_r,ϵ_r) and circumferential strain (e_θ, ϵ_θ) distributions as a function of original radial distance from the pole of domse stretched over a 50.8 mm radius hemispherical punch [4]. More uniform strains during the early stages and a narrower strain peak in the later stage characterizes brass, while steel shows much broader peaks in both radial and circumferential strains.

Strain Distribution Under Biaxial Loading. Distributions of radial and circumferential strains during incremental stretching of A-K steel and brass sheets [4] over a rigid hemispherical punch are shown in Fig. 12. These distributions show that a peak develops in the radial strain distribution early during deformation. Because of strain hardening and frictional resistance on the punch, this peak progressively moves away from the pole and, at some stage, deformation concentrates in it enough to cause localized necking. The interesting fact is that the strain distribution is substantially more uniform from stages 1 through 6 in brass due to its higher n (0.55) compared to steel (n = 0.23). This means that with a smaller peak strain, brass can produce the same size dome as steel at these stages. However, beyond stage 5 for steel, deformation spreads primarily around the peak strained region without much shift in its location, while brass peak continues to move. This behavior for steel arises from its early attainment of diffuse necking strains ($\sim n$), beyond which the spread of deformation is primarily due to its high m (0.012).[7] Brass, on the other hand, reaches diffuse necking much later and rapidly concentrates strain subsequently without any appreciable broadening of the peak (since m = 0).

The result of this effect on the punch load versus displacement plots for these materials is shown in Fig. 13(a). In this case, the inflection point in the curve signals the onset of diffuse necking (roughly a condition of maximum interface pressure), similar to the maximum load in a tensile test. Substantial increase in the punch displacement beyond the diffuse necking point is found to occur for steel, while this amount is less for brass. In a similar manner, dispersion-hardened zinc (m = 0.06) shows a substantial increase in the post-inflection displacement while this effect is very small in 2036-T4 aluminum (m = − 0.005).

The influence of n and m can also be related to the circumferential strain distributions during punch stretching (Fig. 12). Clearly the punch geometry plays a very significant role in these distributions. Circumferential strain, defined as $\epsilon_\theta = \ln (r/r_0)$, where r_0 = original radial distance from center and r = its current value, must increase with ϵ_r in an equal manner near the pole region since this area is relatively flat and constraints are equal from all directions.

Away from the pole, however, the sheet plane inclines closer toward the vertical and a larger increase in ϵ_r can be accommodated with a smaller increase in the radial distance from the punch axis, i.e., with a smaller ϵ_θ. This causes ϵ_θ to drop near the edge. The edge actually deforms in plane strain, while the pole experiences balanced biaxial tension.

While brass shows this behavior well, in the case of steel, the positive m resists rapid strain localization and causes ϵ_θ to rise around the ϵ_r-peak. Observation [12] of a decrease in n with increasing biaxiality (and particularly, a rapid decrease in n with strain under biaxial loading) in the case of brass explains the extreme sharpness of its ϵ_r-peak. Furthermore, the rise in ϵ_θ with ϵ_r allows both A-K steel and dispersion-hardened zinc to shift their strain path to a more positive minor strain (Fig. 13(b)). As seen from Fig. 8, this means moving to a higher point on the forming limit diagram. A positive m therefore improves sheet formability in three ways: (i) by raising the forming limit, (ii) by improving strain distribution around the strain peak, and (iii) by moving to a higher point on the forming limit diagram. In contrast to this, the strain path for brass shown in Fig. 13(b), is closer to plane strain and corresponds to a lower point on the forming limit diagram. Thus the beneficial influence of a high n for brass is somewhat obscured since it helps the strain peak move toward the edge. Its dome height at failure is only 36 mm, in comparison to 32 mm for A-K steel, even though its n is nearly double.

[7] Because strain gradients (and therefore, also gradients in strain-rate) are present during punch stretching from the very beginning of deformation, the distribution of strain is influenced from the very outset, however the effect becomes more pronounced subsequent to diffuse necking.

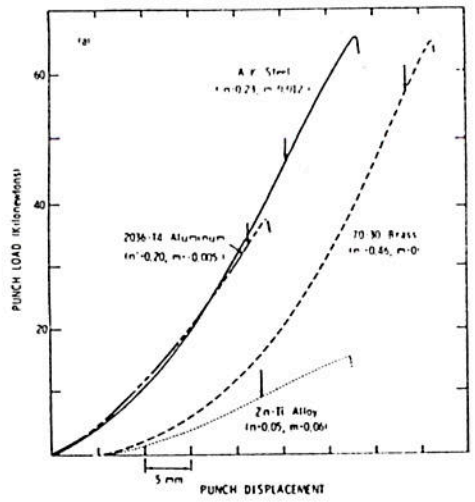

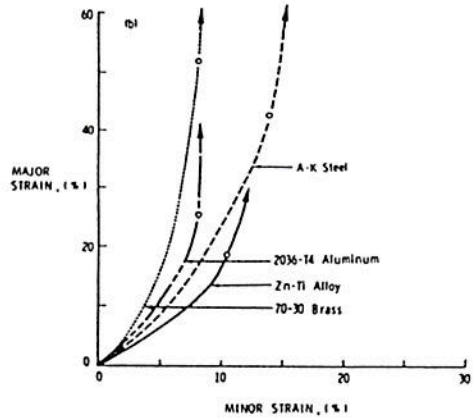

Fig. 13 (*a*) Punch load vs. displacement plots during stretch forming over a 50.8 mm radius punch [4]. The short vertical arrows indicate the points of inflection and roughly signals the onset of diffuse instability (*b*) The strain paths (engineering strains) followed by the peak strain elements during the punch stretching operation (from Fig. 12), shows the points of localized necking (open circle). Major and minor strains refer to radial and circumferential strains, respectively.

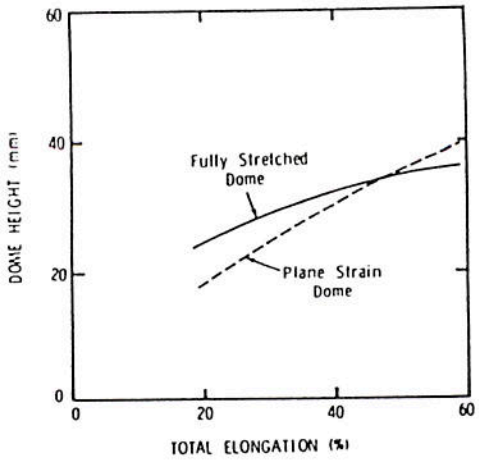

Fig. 14 Dome heights at failure (stretched over 50.8 mm radius hemispherical punch) for sheets plotted as a function of their total elongation (50.8 mm gage length) in a tensile test. [18] Fully stretched case refers to sheets that were clamped with a lock bead all around the periphery to prevent any draw-in. Somewhat narrower blanks, by virtue of slight draw-in produce plane strain states at the failure location.

While the contributions of the two hardening processes on the overall formability of a component (that involves combined stress-states) are rather complex, contributions are derived from both the "uniform" and "post-uniform" components of deformation. Interestingly, the combined role of these constituents in the total tensile elongation (50.8 mm gage length) and dome heights at failure over a 50.8 mm radius punch appear to be similar. Fig. 14 shows a plot of dome height for two different clamping conditions (different failure strain-states) as a function of total tensile elongation for a variety of materials taken from reference [18]. This kind of correlation is considerably stronger than dome height versus n value alone. Part geometry and lubrication conditions would, however, modify such a correlation and formability prediction in such cases would require developing adequate plasticity analyses incorporating these factors.

Influence of Deformation Rate

Since the actual forming operations involve high speed punch motion, its influence on material formability is of importance. Normally, regions of stamping undergoing large deformation also experience increasing rates of strain. It does not appear simple, however, to determine actual strain rates in various parts of a complex stamping although one can estimate that strain rate will lie generally in the reange of 0–10/s.

Increased deformation rate is detrimental to materials in which the primary deformation mechanism is thermal activation, since it does not allow sufficient time for diffusion to occur. In conventional stamping materials, the effect of speed is not well documented; however, it does not appear to be very large. The influence of rate on tensile necking can be understood from an appropriate description of constitutive law. Equation (1) predicts (for $m > 0$) increased load with increased rate of deformation without influencing the necking behavior. However, a better constitutive description for mild steel and 1100-0 aluminum (based on Figs. 7(*b*) and (*c*)) appears to be

$$\sigma(\dot{\epsilon}_2) = \sigma(\dot{\epsilon}_1) + \Delta\sigma \tag{6}$$

where $\sigma(\dot{\epsilon}_1)$ at the lower strain rate is assumed to be described by $K\epsilon^n$ alone and $\Delta\sigma$ is expressable in terms of $\dot{\epsilon}_1$ and $\dot{\epsilon}_2$ by

$$\Delta\sigma = Km' \ln (\dot{\epsilon}_2/\dot{\epsilon}_1) \tag{7}$$

Shown by a schematic construction in Fig. 15(*a*), if the two stress-strain curves (corresponding to two constant rates) are separated by a constant $\Delta\sigma$, their slope ($d\sigma/d\epsilon$) curve will be identical. This means that maximum load will be reached at a smaller strain when the strain rate is increased.

To put this in a quantitative form, if n is known for the lower rate of $\dot{\epsilon}_1$, the maximum load ($d\sigma/d\epsilon = \sigma$) condition requires:

$$(n/\epsilon_u - 1)\epsilon_u^n = (\Delta\sigma/K) = m' \ln (\dot{\epsilon}_2/\dot{\epsilon}_1) \tag{8}$$

With $m' = 0.026$, calculated from Fig. 7(*b*), and $n = 0.23$ for mild steel from reference [4], equation (8) predicts the dependence of strain at maximum load (ϵ_u) as a function of rate (solid line) in Fig. 15(*b*). Experimental data from Chatfield's work [30] is superimposed on this to show that $\epsilon_u(\dot{\epsilon})$ can be predicted well from values of n (at a lower rate) and m. It must be emphasized, however, that m defined by equation (1) is different from the m' value given by equation (7). Finally, since $d\sigma/d\epsilon$ is greater for smaller strains, the stability loss beyond ϵ_u is more gradual at higher $\dot{\epsilon}$. This leads to a broader diffuse neck at higher strain rates. Fig. 15(*b*) also shows total elongation as a function of deformation rate from reference [30]. The effect is less well-defined and normally such data contain a lot of scatter.

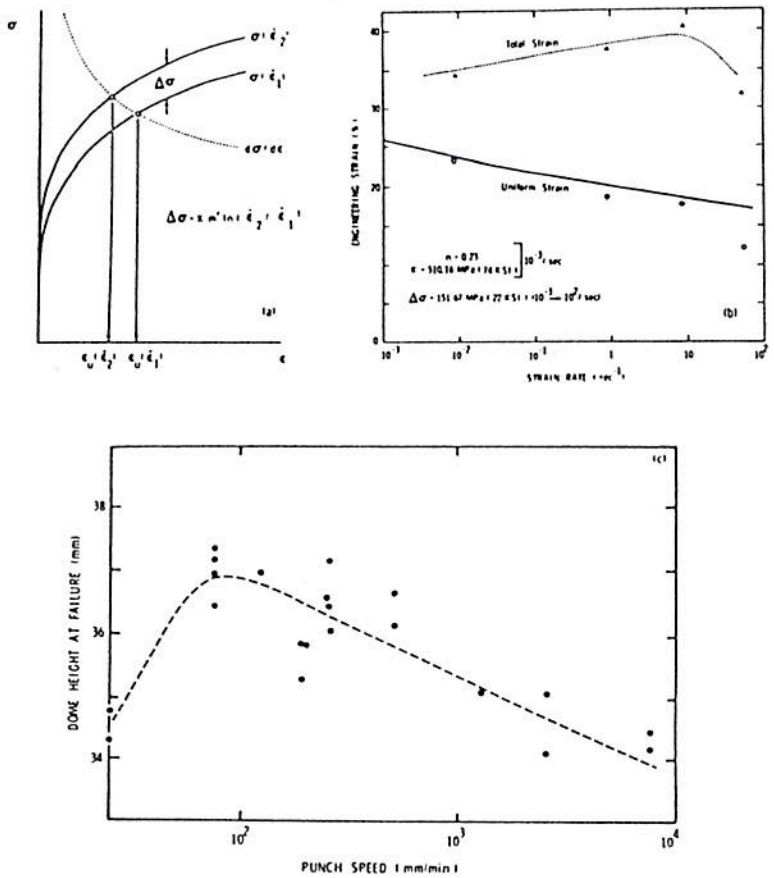

Fig. 15(a) Schematic Considere construction for stress-strain curves at two different strain-rates (differing by a constant $\Delta\sigma$) show that $(d\sigma/d\epsilon)=\sigma$ can be satisfied at a smaller uniform strain for higher strain rates. (b) The prediction of this decrease in uniform strain as a function of strain rate, according to equation (8) in the text, is shown (solid line) for low carbon steel. The $\Delta\sigma$(reference [19]), K and n (reference [4]) values are indicated and comparison is made between the prediction and data (open circles) from reference [30]. (c) The dependence of dome height (50.8 mm radius) on punch speed for fully constrained sheets. The dome height trend is somewhat similar to that of total elongation (Fig. 15 (b)).

Measurements of dome heights (from stretching over a 50.8 mm radius hemispherical punch) as a function of rate for A-K steel also show large scatter (Fig. 15(c)). There is a general trend of some increase initially, followed by a gradual decrease in dome height as a function of punch speed. This kind of behavior may arise from the combined influence of changes in material properties and interface frictional characteristics as a function of speed, and has not been explained in a quantitative manner.

If $\Delta\sigma$ in equation (6) is not constant and increases with strain, ϵ_u would not drop as much, if any, with increase in strain rate. In fact, some elevated temperature studies suggest that ϵ_u increases with rate in Al-5 percent Mg alloy deformed at 300°C [31], and in low carbon steel, deformed between 1000°C and 1200°C [32]. If, on the other hand, $\Delta\sigma$ decreases with strain, an even more rapid drop in ϵ_u would occur with increasing strain rate. All spectrums of behavior are thus possible depending upon the intensity of the thermally activated process (time-dependent) at the prevailing deformation rate and its competition against the athermal hardening (glide based) process.

Conclusions

Detailed examination of sheet stamping materials indicates that the strain hardening exponent, n, is the most important factor in the distribution of strain prior to the onset of diffuse necking. The presence of a small but positive strain-rate sensitivity (m) exercises an important stabilizing influence on the deformation beyond that point. Combination of these effects with a high fracture strain provides low carbon steel with excellent formability. These effects also influence the forming limit, i.e., strain level prior to localized necking in a similar manner. Aluminum alloys, on the other hand, exhibit inferior formability at room temperature, since n diminishes with deformation and m is slightly negative. When $m > 0.02$, as in zinc alloys at room temperature and many metals at elevated temperature, the importance of n on the overall deformation process is reduced, and flow becomes extremely uniform exhibiting some of the characteristics of extended ductility materials. Increase in deformation rate decreases the uniform component of strain in rate-sensitive materials and may either increase or decrease the non-uniform component of deformation. The proper constitutive law, which depends upon the intensity of the thermally activated slip processes, must be characterized adequately, however, to allow predictions of this type.

References

1 Keeler, S. P., "Understanding Sheet Metal Formability," *Machinery*, 1968.

2 KiKuma, T., and Nakazima, K., "Effects of Deforming Conditions and Mechanical Properties on the Stretch Forming Limits of Steel Sheets," *Proceedings of the International Conference on Science and Technology of Iron and Steel*, Suppl. Transactions of the Iron and Steel Institute of Japan, Vol. 11, 1971, pp. 827–831.

3 Wang, N. M., "Large Plastic Deformation of a Circular Sheet Caused by Punch Stretching," *Journal of Applied Mechanics*, Vol. 37, 1970, pp. 431-440.

4 Ghosh, A. K., and Hecker, S. S., "Failure in Thin Sheets Stretched Over Rigid Punches," *Metallurgical Transactions*, Vol. 6A, 1975, pp. 1065–1074.

5 Duncombe, E., "Plastic Instability and Growth of Grooves and Patches in Plates or Tubes," *International Journal of Mechanical Sciences*, Vol. 14, 1972, pp. 325–337.

6 Ghosh, A. K., "A Numerical Analysis of the Tensile Test for Sheet Metals," accepted for publication in *Metallurgical Transactions*, 1977.

7 Penning, P., "Mathematics of the Portevin-Le Chatelier Effect," *Acta Metallurgica*, Vol. 20, 1972, pp. 1169–1175.

8 Hall, E. O., *Yield Point Phenomena in Metals and Alloys*, Plenum Press, New York, 1970.

9 Hill, R., "On Discontinuous Plastic States, With Special Reference to Localized Necking in Thin Sheets," *Journal of the Mechanics and Physics of Solids*, Vol. 1, 1952, pp. 19–30.

10 Ghosh, A. K., "Strain Localization in the Diffuse Neck in Sheet Metals," *Metallurgical Transactions*, Vol. 5, 1974, pp. 1607–1616.

11 Ayres, R. A., "Warm Forming of Aluminum: Dependence of Tensile Ductility on Strain Rate in 5182-0 Alloy," accepted for publication in *Metallurgical Transactions*, 1977.

12 Ghosh, A. K., and Backofen, W. A., "Strain Hardening and Instability in Biaxially Stretched Sheets," *Metallurgical Transactions*, Vol. 4, 1973, pp. 1113–1123.

13 Marciniak, Z., *Aspects of Material Formability*, Lecture Notes at McMaster University, Hamilton, Ontario, Canada, 1974.

14 Ghosh, A. K., and Ayres, R. A., "On Reported Anomalies in Relating Strain-Rate Sensitivity to Ductility," *Metallurgical Transactions 'A,'* Vol. 7A, Oct. 1976, pp. 1589–1591.

15 Woodford, D. A., "Strain-Rate Sensitivity as a Measure of Ductility," Transactions of American Society for Metals, Vol. 62, 1969, pp. 291–293.

16 Honeycomb, R. W. K., *The Plastic Deformation of Metals*, Edward Arnold Publishers, 1968, pp. 228–240.

17 Azrin, M., "The Deformation and Failure of a Biaxially Stretched Sheet," PhD thesis, Massachussetts Institute of Technology, 1970.

18 Ghosh, A. K., "The Effect of Lateral Drawing-In on Stretch Formability," *Metals Engineering Quarterly*, Vol. 15, August 1975, pp. 53–60, 64.

19 Green, S. J., Langan, J. J., Leasia, J. D., and Yang, W. H., "Material Properties Including Strain-Rate Effects, as Related to Sheet Metal Forming," *Metallurgical Transactions*, Vol. 2, 1971, pp. 1813–1820.

20 Hockett, J. E., "On Relating the Flow Stress of Aluminum to Strain, Strain-Rate and Temperature," *Transactions AIME*, Metal Soc., Vol. 239, 1967, pp. 969-976.

21 Rai, G., and Grant, N. J., "On the Measurements of Superplasticity in an Al-Cu Alloy," *Metallurgical Transactions*, Vol. 6A, 1975, pp. 385–390.

22 McGregor Tegart, W. J., *Elements of Mechanical Metallurgy*, The MacMillan Company, New York, 1966, pp. 32–33.

23 Keeler, S. P., "Circular Grid System—A Valuable Aid for Evaluating Sheet Metal Formability," Society of Automotive Engineering Congress, Paper No. 680092, January 1968.

24 Goodwin, G. M., "Application of Strain Analysis to Sheet Metal Forming Problems in the Press Shop," Society of Automotive Engineering Congress, Paper No. 680093, January 1968.

25 Hecker, S. S., "A Simple Technique for Determining Forming Limit Curves," *Sheet Metal Industries*, Vol. 52, 1975, pp. 671–675.

26 Ghosh, A. K., and Hecker, S. S., "Stretching Limits in Sheet Metals: In-Plane vs. Out-of-Plane Deformations," *Metallurgical Transactions*, Vol. 5, 1974, pp. 2161–2164.

27 Swift, H. W., "Plastic Instability Under Plane Stress," *Journal of the Mechanics and Physics of Solids*, Vol. 1, 1952, pp. 1–18.

28 Marciniak, Z., and Kuczynski, K., "Limit Strains in the Process of Stretch-Forming Sheet Metal," *International Journal of Mechanical Sciences*, Vol. 9, 1967, pp. 609–620.

29 Sowerby, R., and Duncan, J. L., "Failure in Sheet Metal in Biaxial Tension," *International Journal of Mechanical Sciences*, Vol. 13, 1971, pp. 217–229.

30 Chatfield, D. A., and Rote, R. R., "Strain Rate Effects on the Properties of High Strength, Low Alloy Steels," Society of Automotive Engineers Congress, Paper No. 740177, Feb. 1974.

31 Arnold, R. R., and Parker, R. J., "Resistance to Deformation of Aluminum and Some Aluminum Alloys; its Dependence on Temperature and Rate of Deformation," *Journal of the Institute of Metals*, Vol. 88, 1959-60, pp. 255–259.

32 Cook, P. M., "True Stress-Strain Curves for Steel in Compression at High Temperature and Strain Rates, for Application to the Calculation of Load and Torque in Hot Rolling," *Proceedings of the Conference on Properties of Materials at High Rates of Strain*, Institution of Mechanical Engineers, London, Session 3, paper 2, 1957.